Journal of Molecular Structure 1052 (2013) 135–145

Contents lists available at ScienceDirect

Journal of Molecular Structure

journal homepage: www.elsevier.com/locate/molstruc

Synthesis, spectroscopy (vibrational, NMR and UV–vis) studies, HOMO–LUMO and NBO analysis of 8-formyl-7-hydroxy-4-methyl-coumarin by ab initio calculations

Hassan Moghanian [a,*], Akbar Mobinikhaledi [b], Roya Monjezi [b]

[a] Department of Chemistry, Dezful Branch, Islamic Azad University, Dezful, Iran
[b] Department of Chemistry, Faculty of Science, Arak University, Arak 38156-8-8349, Iran

HIGHLIGHTS

- 8-Formyl-7-hydroxy-4-methylcoumarin has been synthesized.
- The title compound has been characterized experimentally and theoretically.
- The complete vibrational assignments and spectroscopic analysis were made.
- The geometrical parameters are in agreement with that of similar derivatives.
- NBO, MEP and thermodynamic properties of the title compound have been calculated.

GRAPHICAL ABSTRACT

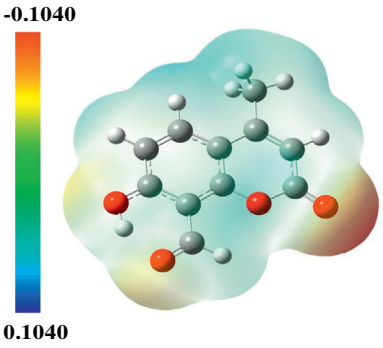

ARTICLE INFO

Article history:
Received 11 May 2013
Received in revised form 21 August 2013
Accepted 21 August 2013
Available online 27 August 2013

Keywords:
8-Formyl-7-hydroxy-4-methylcoumarin
Vibrational spectra
NMR and UV–vis spectra
HOMO–LUMO
NBO analysis

ABSTRACT

In this work, 8-formyl-7-hydroxy-4-methylcoumarin has been synthesized and characterized by elemental analysis, FT-IR, FT Raman, ^{1}H NMR, ^{13}C NMR and UV–vis spectra. The molecular geometry, harmonic vibrational frequencies and gauge including atomic orbital (GIAO) ^{1}H and ^{13}C chemical shift values of the title compound in the ground state have been calculated by using Hartree-Fock (HF) and density functional methods (B3LYP) with 6-311++G(d,p) as basis set. The vibrational assignments of wave numbers were interpreted in terms of potential energy distribution (PED) analysis and the scaled B3LYP/6-311++G(d,p) results show the good agreement with the experimental values. The UV spectra of investigated compound were recorded in the region of 230–500 nm in chloroform solution. The energy and oscillator strength calculated by Time-Dependent Density Functional Theory (TD-DFT) in gas and $CHCl_3$ theoretically and results were compared with experimental observations. The molecular stability arising from hyperconjugative interactions and charge delocalization have been analyzed using natural bond orbital (NBO) analysis. In addition, Frontier Molecular Orbitals (FMO), Molecular Electrostatic Potential (MEP) and thermodynamic properties of the studied compound such as heat capacity (C), entropy (S) and enthalpy changes (H) at different temperatures have been calculated.

* Corresponding author. Tel.: +98 8614173402; fax: +98 8614173406.
E-mail address: moghanian@gmail.com (H. Moghanian).

0022-2860/$ - see front matter © 2013 Elsevier B.V. All rights reserved.
http://dx.doi.org/10.1016/j.molstruc.2013.08.043

1. Introduction

Coumarins or 2H-chromen-2-one derivatives are a biological chemical compounds which are found in several plants, such as lavender, licorice, strawberries, apricots, cherries, cinnamon, and sweet clover. To date, more than 1000 coumarin derivatives have been isolated from plants and microorganisms, and have been produced synthetically for many years for commercial uses [1–4]. Coumarins are an important class of compounds, because of their applications in synthetic chemistry, medicinal chemistry and photochemistry. Many of these compounds have proved to be active as, antimicrobial [5,6], antibacterial [7,8], antifungal [9], anti inflammatory [10], anticoagulant [11], antitumor [12] and free radical scavenging activity especially the superoxide anions generated by activated neutrophils [13]. Coumarins are excellent laser dyes at near-ultraviolet to green wavelength due to its strong absorption cross sections and large radiative yields [14]. In addition, coumarin derivatives have been used as fluorescent probes of pH [15,16], for detection of nitric oxide [17], nitroxide [18], and hydrogen peroxide [19,20].

The vibrational spectroscopic techniques (IR and Raman spectroscopy) are noninvasive methods yielding molecular fingerprint information for the investigation of biological systems. In the vibrational analysis of polyatomic complex molecules, analysis of the assignment of vibrations is supported by quantum chemical calculations, because there are many couplings between vibrations. Theoretical calculation method is a powerful tool for molecular design, and can help unambiguous identification of vibrational modes as well as the bonding and structural features of complex organic molecular systems and in comparision with experimental molecular modification are not only low-cast but time-saving. According to previous literature, vibrational spectra for the parent coumarin and its derivatives such as dihydro-, 6-methyl and 7-methylcoumarins [21–24], 3-acetylcoumarin [25], 3-(bromoacetyl)coumarin [1], 6-methyl-4-bromomethylcoumarin [26], 7-methyl-4-bromomethyl coumarin [27], 4-hydroxy-1-thiocoumarin [28], 3-cyano-4-methylcoumarin [29], 7-hydroxycoumarin [30] and 3-acetyl-7-methoxycoumarin [31] have been reported.

A literature survey revealed that, there have been no reports on the electronic, vibrational and structural properties of 8-formyl-7-hydroxy-4-methylcoumarin. Therefore, due to the above biological importance, in the present work, the Infrared and Raman spectral analysis, NMR and UV spectral and other structural parameters of 8-formyl-7-hydroxy-4-methylcoumarin have been investigated using Hartree-Fock (HF) and Density Functional Theory. Complete vibrational assignments of wave numbers of the molecule were performed by combining the experimental and theoretical information using potential energy distribution (PED) analysis. The energy and oscillator strength calculated by TD-DFT calculations complements with the experimental findings. The experimental and theoretical results support each other, and the calculations are valuable for providing a reliable insight into the vibrational spectra and the molecular properties.

2. Experimental section

2.1. Synthesis

8-Formyl-7-hydroxy-4-methylcoumarin was prepared in two steps according to the well-known literature procedure with slight modifications [32,33]. The synthetic route is shown in supplementary Scheme S1. To a mixture of resorcinol (4.4 g, 40 mmol) and ethyl acetoacetate (5.2 g, 40 mmol), pTSA (0.36 g, 2.0 mmol) was added and the reaction mixture was irradiated using the microwave oven for 30 s at 450 W power. After removing from the microwave oven, the reaction mixture was allowed to cool down to room temperature. Then, a mixture of EtOH–H_2O (1:1) was added to it, the suspension was stirred for 5 min and the precipitate filtered and dried to afford 6.68 g of 7-hydroxy-4-methylcoumarin (yield 95%; mp: 184–186 °C), that used in the next step without further purification.

A mixture of 7-hydroxy-4-methylcoumarin (5 g, 28.4 mmol) and hexamine (5.6 g, 40 mmol) in glacial acetic acid (90 mL) were heated for 4 h. Then, hexamine (5.6 g, 40 mmol) was added to the reaction mixture and heated for another 4 h. Upon completion of the reaction (monitored by TLC), 70 mL of 20% HCl was added in and the mixture was further heated for 40 min. Then, the reaction mixture was cooled to room temperature and extracted with ether twice (50 mL × 2). The combined organic layer was concentrated under reduced pressure and the crude product was recrystallized from ethanol to afford 1.04 g of 8-formyl-7-hydroxy-4-methylcoumarin (yield 18%; mp: 145–146 °C). FT-IR (in KBr pellet) υ_{max} (cm^{-1}): 3063, 1746 (C=O of lactone), 1647 (C=O of formyl), 1595, 1390, 1300 (C–O), 1167 and 1074 (C–O); ^{1}H NMR (400 MHz, $CDCl_3$): δ = 12.12 (s, 1H, OH), 10.53 (s, 1H, CHO), 7.67 (d, *J* = 8.8 Hz, 1H, Ar. CH), 6.83 (d, *J* = 8.4 Hz, 1H, Ar. CH), 6.13 (s, 1H, Vinyl CH), 2.36 (s, 3H, CH_3); ^{13}C NMR (100 MHz, $CDCl_3$): δ = 193.4 (C=O of formyl), 165.2 (C–OH), 159.2, 156.1 (C=O of lactone), 152.8, 133.0, 114.3, 112.4, 112.0, 108.6, 19.0 (CH_3); Anal. Calcd. For $C_{11}H_8O_4$: C, 64.71; H, 3.95; found: C, 64.65; H, 3.92.

2.2. Measurement of FTIR and FT-Raman spectra

The FTIR spectrum of the sample was recorded on a Unicom Galaxy Series FT-IR 5000 spectrophotometer in the region 4000–400 cm^{-1} using pressed KBr discs. The spectra were collected with a resolution of 1 cm^{-1} by signal averaging the results of 15 scans. FT-Raman spectrum of the sample was recorded using 1064 nm line of Nd:YAG laser as excitation wave length in the region 4000–80 cm^{-1} on a Bruker RFS 100/S FT-Raman. The detector is a liquid nitrogen cooled Ge detector. Five hundred scans were accumulated at 4 cm^{-1} resolution using a laser power of 100 mW.

2.3. Measurement of NMR and UV–vis spectra

The ^{1}H and ^{13}C NMR spectra were recorded on a Brucker Avance spectrometer operating at 400 and 100 MHz for proton and carbon-13, respectively in $CDCl_3$ with TMS as an internal standard. The UV–vis absorption spectrum of the compound was recorded in chloroform solution using a Perkin–Elmer Lambda spectrophotometer in the spectral region of 230–500 nm, using 1 cm path quartz cells.

3. Computational details

All of the ab initio calculations for this work have been performed at HF and DFT (B3LYP) methods with 6-311++G(d,p) basis sets using the Gaussian 09 W program [34]. The geometry optimization of the title compound and corresponding energy and harmonic vibrational frequencies were calculated at different level of theories with 6-311++G(d,p) basis set by assuming Cs point group symmetry. The absence of imaginary frequency verified that optimized geometry for the title molecule was true minima on the potential energy surface at their respective levels of theory. As a result, the optimized geometrical parameters, energy, fundamental vibrational frequencies, IR intensity, Raman activity, the atomic

charges, dipole moments and other thermodynamical parameters were calculated theoretically. In order to improve the calculated values in agreement with the experimental values, it is necessary to scale down the calculated harmonic frequencies Hence, the vibrational frequencies calculated at HF level are scaled by 0.9067 and the range of wave numbers above 1700 cm^{-1} are scaled by 0.958 and below 1700 cm^{-1} scaled by 0.983 for B3LYP [35,36]. Furthermore, the theoretical vibrational spectra of the title compound are interpreted by means of potential energy distribution (PED) using VEDA program [37]. Gauss view program [38] has been considered to get visual animation and also for the verification of the normal modes assignment.

The Raman activities (S_{Ra}) calculated with Gaussian 09 W program [34] converted to relative Raman intensities (I_{Ra}) using the following relationship derived from the intensity theory of Raman scattering [39,40].

$$I_i = \frac{f(v_0 - v_i)^4 S_i}{v_i[1 - \exp(-hcv_i/kT)]}$$

where v_0 is the laser exciting wave number in cm^{-1} (in this work, we have used the excitation wave number = 9398.5 cm^{-1}, which corresponds to the wavelength of 1064 nm of a Nd:YAG laser), v_i is the vibrational wave number of the ith normal mode (cm^{-1}), while S_i is the Raman scattering activity of the normal mode v_i. f (is a constant equal to 10^{-12}) is a suitably chosen common normalization factor for all peak intensities. h, k, c and T are Planck, Boltzmann constant, speed of light and temperature in Kelvin, respectively.

The NBO calculations [41] were performed using NBO 5.0 program as implemented in the Gaussian 09 W [34] package at the DFT/B3LYP/6-311++G(d,p) level. The electronic properties, such as HOMO–LUMO energies, dipole moment, absorption wavelengths, and oscillator strengths were calculated using B3LYP method of the time-dependent DFT (TD-DFT) [42–45] and 6-311++G(d,p) basis set, based on the optimized structure.

The ^{13}C and ^{1}H NMR isotropic shielding were calculated with the GIAO method [46,47] using the optimized molecule geometry. The isotropic shielding values were used to calculate the isotropic chemical shifts (δ) with respect to tetramethylsilane using the relation $\delta_{iso} = \sigma_{TMS} - \sigma_{iso}$, where δ_{iso} isotropic chemical shift and σ_{iso} isotropic shielding constant.

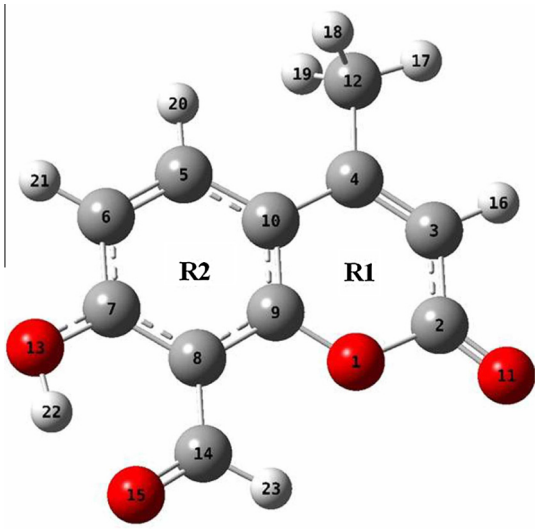

Fig. 1. Molecular structure of 8-formyl-7-hydroxy-4-methylcoumarin along with numbering of atoms.

4. Results and discussion

4.1. Molecular geometry

A complete geometrical optimization was performed within the C_S point group symmetry and the most stable conformer of 8-formyl-7-hydroxy-4-methylcoumarin with numbering of the atoms is shown in Fig. 1.

The oxygen atom of the –OH group and the formyl (–CHO) oxygen atom of the compound are exactly in the plane of the ring. This is confirmed by the corresponding dihedral angles C_7–C_8–C_{14}–O_{15} (0°) and C_{14}–C_8–C_7–O_{13} (0°). The energy barrier of rotation around the O_{13}–C_7 bond was calculated for the B3LYP/6-311G++(d,p) method. The potential energy scans of the internal rotations about the H_{22}–O_{13}–C_7–C_6 single bond was obtained by allowing the ring-OH angle to vary every 10° from 0° to 360° (Fig. 2.). The energy profile obtained from DFT method (Fig. 2) has shown three local minima at 0°, 180° and 360° and two maxima near 90° and 270° which predicts that the conformer at 0° (or 360°) is the most stable conformer of 8-formyl-7-hydroxy-4-methylcoumarin. The energy difference between the most stable (0°) and the second stable (180°) conformations is 54.63 kJ mol^{-1}.

The global minimum energy obtained for structure optimization of 8-formyl-7-hydroxy-4-methylcoumarin with 6-311++G(d,p) basis set is −725.10295 a.u. for DFT/B3LYP and −720.86264 a.u. for HF method. The difference in amount energy between the methods is 4 a.u. only. The optimized values of bond lengths and bond angles are reported in Table 1. Since the crystal structure of 8-formyl-7-hydroxy-4-methylcoumarin is not available in the literature. Therefore, the optimized structure of the title compound is compared with other analogous compounds such as 8-formyl-7-tosyloxy-4-methylcoumarin [48]. The experimental C–C bond lengths fall in the range of 1.334–1.499 Å and the optimized C–C bond lengths for 8-formyl-7-hydroxy-4-methylcoumarin fall in the range of 1.3575–1.5034 Å by DFT/B3LYP and 1.3365–1.5035 Å by HF method. From the analysis of geometric parameters, we notice that such differences between calculated and measured values. These discrepancies can be explained by the fact that the calculations assume an isolated molecule whereas the experimental result corresponds to interacting molecules in the crystal lattice and also, these parameters depend on the method and the basis set used in the calculations. HF and DFT calculations show shortening of bond length in C_3–C_4 1.3365 Å and 1.3575 Å respectively, which confirms the presence of double bond character. Several authors have explained the changes in the frequency or bond length of C–H bond on substitution due to a change in the charge distribution on the carbon atom of the benzene ring. In the title molecule, hydroxyl and formyl groups interact with the systems. This interaction can affect regular hexagonal structure as evident from calculated bond angles from Table 1. For example,

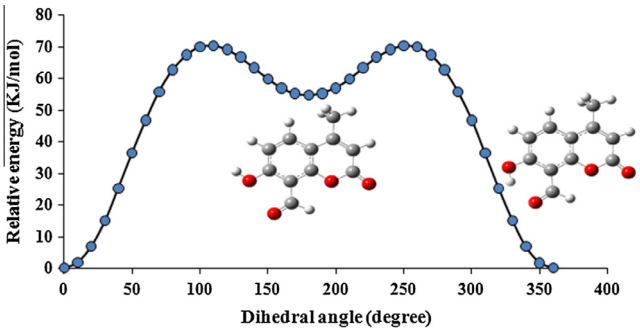

Fig. 2. Scan of potential energy for the internal rotations about the H_{22}–O_{13}–C_7–C_6.

Table 1
Calculated optimized parameter values of 8-formyl-7-hydroxy-4-methylcoumarin.

Bond lengths (Å)	Exp.[a]	HF/6- 311++G(d,p)	B3LYP/6-311++G(d,p)	Bond angles (°)	Exp.[a]	HF/6-311++G(d,p)	B3LYP/6-311++G(d,p)
R(1, 2)	1.383 (2)	1.3635	1.4124	A(2,1,9)	121.95 (13)	123.83	122.84
R(1, 9)	1.3696 (19)	1.3396	1.3524	A(1,2,3)	116.45 (15)	116.03	115.41
R(2, 3)	1.440 (2)	1.4569	1.4467	A(1,2,11)	116.59 (16)	117.92	116.92
R(2, 11)	1.200 (2)	1.1778	1.2004	A(3,2,11)	126.95 (16)	126.06	127.67
R(3, 4)	1.334 (2)	1.3365	1.3575	A(2,3,4)	123.55 (16)	122.07	123.04
R(3, 16)	0.9300	1.0723	1.0821	A(2,3,16)	118.2	115.21	115.14
R(4, 10)	1.452 (2)	1.4598	1.4497	A(4,3,16)	118.2	122.73	121.82
R(4, 12)	1.499 (2)	1.5035	1.5034	A(3,4,10)	118.42 (15)	118.85	119.01
R(5, 6)	1.369 (3)	1.3666	1.3774	A(3,4,12)	121.31 (17	121.21	120.81
R(5, 10)	1.397 (2)	1.4036	1.4130	A(10,4,12)	120.27 (16)	119.93	120.18
R(5, 20)	0.9300	1.0741	1.0832	A(6,5,10)	121.44 (17)	122.20	122.28
R(6,7)	1.378 (3)	1.3997	1.4056	A(6,5,20)	119.3	118.54	118.74
R(6,21)	0.9300	1.0729	1.0823	A(10,5,20)	119.3	119.25	118.98
R(7,8)	1.390 (2)	1.4008	1.4181	A(5,6,7)	119.21 (17)	119.69	119.79
R(7,13)	1.407 (2)	1.3179	1.3320	A(5,6,21)	120.4	121.69	121.65
R(8,9)	1.399 (2)	1.4028	1.4130	A(7,6,21)	120.4	118.67	118.57
R(8,14)	1.476 (3)	1.4716	1.4574	A(6,7,8)	122.83 (17)	120.16	120.13
R(9,10)	1.395 (2)	1.3828	1.4017	A(6,7,13)	119.04 (16)	117.25	118.40
R(12,17)	0.9600	1.0860	1.0899	A(8,7,13)	118.08 (17)	122.58	121.47
R(12,18)	0.9600	1.0860	1.0942	A(7,8,9)	116.10 (16)	118.16	118.38
R(12,19)	0.9600	1.0860	1.0942	A(7,8,14)	122.41 (17)	121.05	120.08
R(13,22)	-	0.9522	0.9903	A(9,8,14)	121.43 (16)	120.79	121.55
R(14,15)	1.137 (3)	1.1979	1.2308	A(1,9,8)	116.03 (14)	116.31	116.54
R(14,23)	0.9300	1.0862	1.0980	A(1,9,10)	121.05 (14)	121.17	121.45
Intramolecular H bond lengths and angles				A(8,9,10)	122.91 (15)	122.52	122.01
				A(4,10,5)	124.09 (16)	124.68	124.33
R(15,22)		1.8369	1.7026	A(4,10,9)	118.47 (15)	118.05	118.25
A(13, 22, 15)		141.51	146.90	A(5,10,9)	117.44 (16)	117.26	117.42
A(22, 15, 14)		101.14	101.02	A(4,12,17)	109.5	110.63	110.87
Comparison of bond lengths				A(4,12,18)	109.5	110.66	111.03
$R_{exp.} = 1.3672\ R_{HF} - 0.5117$		$R^2 = 0.9629$	RMSD = 0.0429	A(4,12,19)	109.5	110.66	111.03
$R_{exp.} = 1.3948\ R_{B3LYP} - 0.5623$		$R^2 = 0.9726$	RMSD = 0.0369	A(17,12,18)	109.5	108.44	108.23
				A(17,12,19)	109.5	108.44	108.23
				A(18,12,19)	109.5	107.92	107.31
				A(7,13,22)	–	110.60	107.71
Comparison of bond angles				A(8,14,15)	–	123.11	122.83
$A_{exp.} = 0.9243\ A_{HF} + 8.8961$	$R^2 = 0.8832$	RMSD = 1.6432		A(8,14,23)	–	116.45	117.10
$A_{exp.} = 0.9260A_{B3LYP} + 8.7316$	$R^2 = 0.9006$	RMSD = 1.5272		A(15,14,23)	–	120.44	120.07

RMSD – Root mean square deviation.
[a] Taken from Ref. [48].

C_5–C_{10}–C_9 and C_6–C_5–C_{10} angles are 117.26° and 122.20° by HF and 117.42° and 122.28° by B3LYP method. In addition, due to the electronic repulsion of O_{11} atom attached to the C_2 with that of O_1, a significant deviation from trigonality in bond angle C_3–C_2–O_{11} (126.06° for HF and 127.67° for B3LYP) is observed. As seen in Table 1, the B3LYP values ($R^2_{bondlength} = 0.9726$ and $R^2_{bondangle} = 0.9006$) were found to be in good agreement with the experimental values.

The structure has strong intramolecular hydrogen bond between the oxygen atom of the formyl group and the proton of the hydroxyl group. The intramolecular H bond length ($H_{22}\cdots O_{15} = 1.7026$ Å) and the stability arising from this interaction (Fig. 2) in DFT/B3LYP confirm the presence of intramolecular attractive force between the hydrogen (H_{22}) and the formyl oxygen atom (O_{15}).

4.2. Vibrational analysis

The 8-formyl-7-hydroxy-4-methylcoumarin consists of 23 atoms, and so it has 63 normal vibrational modes. On the assumption of Cs symmetry point group, the number of vibrational modes of the 63 fundamental vibrations is divided into 42A′ + 21A″. The vibrations of the A′ species are in plane modes and those of the A″ species are out-of plane modes. All vibrations are active both in Raman and infrared absorptions. It should be noted that the calculations were made for a free molecule in vacuum, while experiments were performed for solid phase. Thus, there are some deviations between the observed and calculated frequencies, which may be attributed to a crystal field effect, giving rise to intermolecular interactions. In order to improve the agreement between the calculated and the experimentally observed values, the calculated harmonic frequencies have been scaled down via introduction of scaling factors.

The experimental assignments of FT-IR and FT-Raman for several vibrations, unscaled and scaled vibrational frequencies using HF and B3LYP method with 6-311++G(d,p) basis set, IR theoretical and intensities, Raman activity and Raman intensities of 8-formyl-7-hydroxy-4-methylcoumarin were reported in Table 2 and Supplementary Table S1. The experimental FTIR and FT-Raman spectra with corresponding theoretically simulated FTIR and FT-Raman spectra for 8-formyl-7-hydroxy-4-methylcoumarin are shown in Figs. 3 and 4, respectively, where the calculated infrared intensities and relative Raman intensities are plotted against the vibrational frequencies.

The specific assignment to each frequency is attempted through potential energy distribution (PED) using VEDA program [37]. Mostly the maximum contribution is agreed to be the most significant mode. Since the scaled wave numbers following B3LYP/6-311++G(d,p) method are found closest to experimental data than

Table 2
Experimental and calculated (unscaled and scaled) B3LYP/6-311G++(d,p) level vibrational frequencies (cm^{-1}) and probable assignments of 8-formyl-7-hydroxy-4-methylcoumarin.

No.	Symm. species	Exp. frequencies [a]		B3LYP/6-311++G(d,p) [b]					Characterization of normal modes with PED (%) [c]
		FTIR	FT-Raman	Unscaled	Scaled	I^{IR}	S^a	I^{Ra}	
1	A′	–	–	3296	3157	311.3	79.9	33.6	υ OH (99)
2	A′	–	–	3208	3073	1.5	177.5	81.2	υ_s CH R2 (99)
3	A′	3063 (w)	3067 (vw)	3206	3071	0.3	124.6	57.1	υ CH R1 (99)
4	A′	–	3031 (vw)	3189	3055	3.1	57.2	26.7	υ_{as} CH R2 (100)
5	A′	2995 (vw)	2982 (vw)	3124	2993	15.2	77.1	38.2	υ_{as} CH_3 (95)
6	A′	–	–	3081	2952	7.8	68.5	35.4	υ_{as} CH_3 (100)
7	A′	–	–	3038	2911	23.5	53.3	28.7	υ CH formyl (99)
8	A′	2904 (vw)	2907 (w)	3031	2903	8.6	211.1	114.5	υ_s CH_3 (95)
9	A′	1746 (vs)	1726 (s)	1815	1739	754.1	153.5	279.7	υ CO lactone (82)
10	A′	1647 (vs)	1642 (m)	1695	1667	520.5	102.2	212.3	υ CO formyl (69)
11	A′	–	–	1665	1637	84.4	30.0	64.4	υ CC (57)
12	A′	1595 (s)	1594 (vs)	1628	1600	291.0	138.6	310.5	υ CC (56)
13	A′	–	–	1615	1588	94.5	133.7	303.8	υ CC (57)
14	A′	1480 (m)	1484 (w)	1514	1489	52.2	14.6	37.3	υ CC (36) + δ CH R2 (28)
15	A′	–	–	1492	1467	6.6	11.9	31.2	δ CH_3 deformation (85)
16	A″	1433 (w)	1436 (w)	1484	1459	11.0	9.1	24.1	δ CH_3 deformation(90)
17	A′	–	–	1463	1438	66.6	40.3	109.2	υ CC (49) + δ CH formyl (13)
18	A′	1390 (s)	1388 (s)	1432	1408	47.8	90.9	255.9	δ CH formyl (71)
19	A′	–	–	1421	1397	65.5	19.3	55.1	υ CC (12) + δ CH_3 deformation (66)
20	A′	1379 (m)	–	1408	1384	110.5	88.0	255.1	δ_s CH_3 deformation, umbrella (55)
21	A′	1352 (w)	1352 (m)	1381	1358	49.5	8.0	23.7	υ CC (13) + δ OH (31)
22	A′	1300 (s)	1310 (m)	1356	1333	1.5	62.2	192.3	υ CO (51)
23	A′	–	–	1328	1306	235.9	62.8	200.9	υ CC (58)
24	A′	1248 (vw)	1258 (vw)	1272	1250	21.1	8.2	28.3	δ CH R1, R2 (42) + υ CC_{CH3} (10)
25	A′	1228 (m)	–	1249	1228	82.4	6.5	22.9	δ CH R1 (23) + υ CC_{CH3} (34)
26	A′	1184 (m)	–	1203	1182	51.3	4.3	16.0	δ CH R2 (39) + υ CC (35)
27	A′	1167 (s)	1167 (vs)	1161	1141	33.5	82.1	326.9	υ CC (39) + δ OCO (10)
28	A′	1136 (vw)	–	1142	1123	0.4	25.7	105.2	υ CC (43) + δ CH R2 (18)
29	A′	1074 (s)	1077 (m)	1084	1065	115.9	27.6	122.2	υ CO (65)
30	A″	1037 (vw)	1040 (vw)	1059	1041	2.0	0.4	2.0	δ CH_3 Rocking (81)
31	A″	1010 (vw)	1013 (w)	1024	1007	6.9	5.1	24.8	δ CH_3 Rocking (72)
32	A″	–	–	1022	1005	1.6	0.9	4.4	γ CH formyl (94)
33	A″	929 (m)	933 (m)	971	955	0.5	0.2	1.1	γ CH R2 (91)
34	A′	–	–	933	917	30.0	4.7	26.0	υ CO (58)
35	A″	868 (m)	–	872	857	30.0	0.8	4.6	γ CH R1 (81)
36	A″	827 (m)	833 (w)	850	835	42.7	0.7	4.5	γ OH (81)
37	A′	–	–	828	814	34.1	7.5	49.5	δ OCO (49) + υ C–O (12)
38	A′	802 (vw)	–	825	811	83.5	0.2	1.1	γ CH R2 (77)
39	A″	773 (m)	772 (vw)	803	790	16.6	1.6	10.8	δ CCC(62) + δ OCO (12)
40	A′	746 (m)	751 (s)	757	744	25.5	19.8	149.6	δ CCO formyl (41) + υ CC (15)
41	A″	717 (w)	721 (vw)	735	723	16.4	0.4	3.2	τ COCC R1 (81)
42	A′	696 (w)	700 (m)	707	695	8.7	11.6	97.1	δ CCC R2 (61)
43	A″	–	–	696	684	0.1	0.2	1.9	τ CCCC R2 (81)
44	A″	650 (vw)	655 (vw)	649	638	3.7	0.1	0.9	τ CCCC R2 (82)
45	A′	592 (m)	592 (w)	597	587	16.4	1.0	10.1	δ OCO (68)
46	A″	559 (vw)	560 (m)	558	548	2.2	1.2	14.5	τ $CCCC_{CH3}$ (84)
47	A′	542 (w)	543 (s)	545	536	4.4	17.4	211.6	δ CCO formyl (21) + υ CC (47)
48	A″	475 (m)	475 (m)	483	475	32.9	4.5	64.8	δ CCO hydroxy (69)
49	A′	–	–	469	461	2.0	0.8	11.4	τ CCCC R2 (74)
50	A′	455 (w)	457 (m)	460	453	7.2	4.2	65.9	δ CCC R1 (70)
51	A′	428 (vw)	430 (s)	429	422	7.4	15.7	270.2	υ CC (10) + δ COC (70)
52	A′	–	390 (m)	386	380	0.6	7.4	148.5	δ CCC R2 (52)
53	A′	–	317 (w)	331	326	3.6	0.3	8.2	δ CCC R2 (71)
54	A″	–	292 (w)	302	296	0.6	0.3	8.6	τ CCCO formyl (83)
55	A′	–	–	291	286	3.1	2.9	92.4	δ CCC_{CH3} (71)
56	A″	–	–	272	268	3.0	0.1	3.7	τ CCCO (84)
57	A″	–	220 (m)	218	214	7.0	1.9	96.9	τ CCCO formyl (85)
58	A′	–	197 (m)	205	202	0.1	0.8	43.1	τ $CCCC_{CH3}$ (90)
59	A″	–	–	190	187	2.2	2.1	132.4	δ CCO (56)
60	A″	–	150 (w)	168	166	0.0	0.3	22.6	τ CH_3 (92)
61	A″	–	–	134	132	0.0	0.2	17.4	τ CCCO hydroxy (80)
62	A″	–	97 (s)	97	96	0.8	0.1	17.8	τ COCC R1 (81)
63	A″	–	–	65	64	1.6	0.1	62.2	τ CCOC R1 (79)
δ_{Exp} = 0.9934 $\delta_{Scal.}$ + 4.7062				R^2 = 0.9997	RMSD = 12.388				

[a] s: strong; vs: very strong; m: medium; w: weak; vw: very weak.
[b] IIR: Infrared intensity; S^a: Raman activity; I^{Ra}: Raman intensity.
[c] υ: stretching; δ: in-plane bending; γ: out-of-plane bending; τ: torsion; s: symmetry; as: asymmetry; R1: lactone ring; R2: benzene ring.

the results obtained using other methods, so only the PEDs from this set of data are discussed in detail.

4.2.1. O–H vibrations

The O–H group vibrations are likely to be the most sensitive to the environment and move to lower avenues usually with increased intensity and band broadening in the hydrogen bonded species. The non-hydrogen bonded or free hydroxyl group absorbs strongly in the region 3700–3500 cm^{-1} [49], while the existence of intermolecular hydrogen bond formation can lower the O–H stretching wave number to the 3500–3200 cm^{-1} [50]. The computed wave number for the O–H stretching is at 3578 cm^{-1} (mode No. 1) by HF/6-311++G(d,p) and 3157 cm^{-1} by B3LYP/6-311++G(d,p) method with PED contribution of 99%, while in the experimental FT-IR spectrum no clear peak observed, probably due to the presence of strong intramolecular hydrogen bonding between the O–H and oxygen atom of the formyl group. The O–H in-plane vibrations are strongly mixed with C–H in-plane and C–C stretching vibrations, in this work, experimentally observed medium band in Raman at 1352 cm^{-1} and weak observed band at 1352 cm^{-1} in IR spectrum has been assigned to O–H in-plane bending vibration which shows good agreement with computed wave number at 1358 cm^{-1} (mode No. 21) by B3LYP/6-311++G(d,p) method with PED contribution of 31%. The O–H out-of-plane bending vibrations is appears as broad region around 700–600 cm^{-1}. The position of the band is dependent on the strength of the hydrogen bond, stronger the hydrogen bond, the higher the wave number. The medium band observed at 827 cm^{-1} in FT-IR spectrum and weak band observed at 833 cm^{-1} in FT-Raman spectrum are assigned to O–H out-of-plane bending vibrations, which shows good correlation with computed wave number at 835 cm^{-1} by B3LYP and at 830 cm^{-1} by HF method with PED contribution of 81%.

4.2.2. C–H and CH_3 vibrations

Aromatic compounds commonly exhibit multiple weak bands in the region 3100–3000 cm^{-1} due to aromatic C–H stretching vibrations [51–53]. The weak bands appeared at 3063 cm^{-1} in FTIR spectrum and 3067 and 3031 cm^{-1} in FT-Raman spectrum are assigned to C–H stretching vibrations. The corresponding bands for these vibrations were calculated at 3073, 3071, and 3055 cm^{-1} in B3LYP method and at 3060, 3058, and 3040 cm^{-1} in HF method. As evident from the PED column, they are pure vibrations almost contributing to 99% and it is found well with related work [30]. The C–H in-plane bending vibrations appear in the region 1400–1050 cm^{-1} and C–H out of plane bending vibrations in the range of 1000–675 cm^{-1} [54,55]. The bands corresponding to the C–H in-plane bending vibrations are identified in 8-formyl-7-hydroxy-4-methylcoumarin at 1248, 1228, 1184 cm^{-1} in infrared spectra and 1258 cm^{-1} in Raman spectra. The corresponding calculated modes are dominated by C–H in plane bending and coupled with C–C stretching. The computed wave numbers at 1250, 1228, 1182 cm^{-1} and 1239, 1202, 1173 cm^{-1} by B3LYP and HF method respectively, are assigned to C–H inplane bending vibrations. The out of plane bending vibrations in 8-formyl-7-hydroxy-4-methylcoumarin are observed as medium band at 933 cm^{-1} in Raman spectrum and the corresponding IR bands are at 929, 868 and 802 cm^{-1}, respectively. It is consistent with the computed wave numbers of 989, 857, 797 and 955, 857, 811 cm^{-1} by HF and B3LYP methods respectively, with PED contribution of 77–91%. In addition, the strong band observed at 1390 cm^{-1} in FT-IR and the strong band observed at 1388 cm^{-1} in FT-Raman are assigned to be C–H in plane bending vibration of formyl group. The theoretically computed HF and B3LYP values at 1402 cm^{-1} and 1408 cm^{-1} respectively, with PED contribution of 71% show good agreement with experimental data. The C–H stretching and out of plane bending vibrations of formyl group not observed in experimental FT-IR and FT-Raman spectrum and the theoretically calculated wave numbers are presented in Table 2 and Supplementary Table S1.

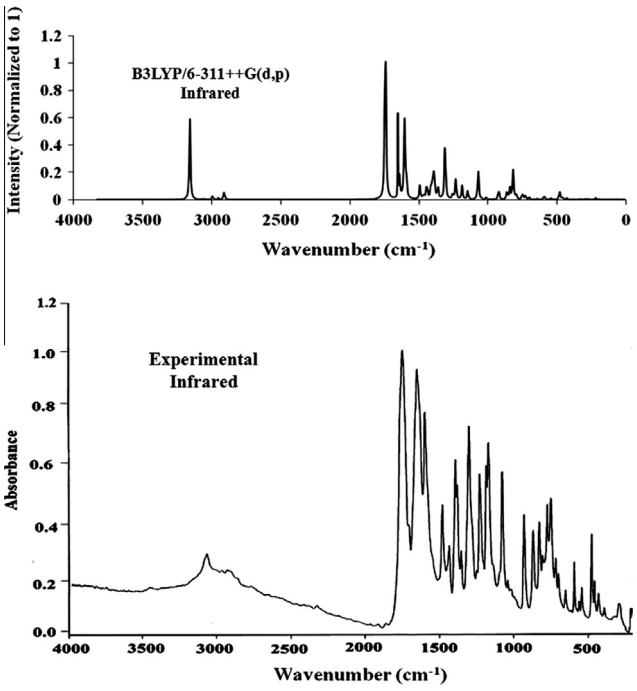

Fig. 3. Comparison of observed and calculated FT-IR spectra of 8-formyl-7-hydroxy-4-methylcoumarin.

The CH_3 group commonly gives rise to nine internal modes of vibration such as three stretching, three bending, two rocking and a single torsional mode. The asymmetric and symmetric stretching modes of CH_3 group normally appear at lower frequency region 2850–3000 cm^{-1} [54,55]. The asymmetric stretching mode is observed as a very weak band as out of phase vibration (indicated as υ_{as} CH_3 Table 2) at 2995 cm^{-1} in IR and a very weak band at 2982 cm^{-1} in Raman. The weak Raman band at 2907 cm^{-1} and a very weak band in IR at 2904 cm^{-1} are assigned to methyl symmetric stretching vibration. The calculated wave numbers of the above modes are 2993 cm^{-1} (95%) and 2903 cm^{-1} (95%) respectively by B3LYP/6-311++G(d,p) level for methyl asymmetric and symmetric modes. The asymmetric and symmetric bending vibrations of methyl groups normally appear in the region 1465–1410 and 1390–1370 cm^{-1} respectively [52,55–57]. The weak band at 1433 cm^{-1} in IR and 1436 cm^{-1} in Raman is attributed to the CH_3 asymmetric bending mode. The corresponding theoretically computed HF and B3LYP values at 1453 cm^{-1} and 1459 cm^{-1} respectively, for CH_3 asymmetric bending with PED contribution of 90% showed good agreement with recorded spectrum. The theoretically value predicted by HF and B3LYP methods at 1366 and 1384 cm^{-1} are assigned to CH_3 symmetric bending vibration of CH_3 group and shows good agreement with the recorded value of 1379 cm^{-1} in FT-IR with PED contribution of 55%.

The rocking vibrations of CH_3 modes usually appear in the region 1070–1010 cm^{-1} [54,55]. The very weak bands observed at 1037 and 1010 cm^{-1} in FTIR spectrum and 1040 and 1013 cm^{-1} in FT-Raman spectrum are assigned to CH_3 rocking vibrations (indicated as δ CH_3 rocking in Table 2). The theoretically computed values by HF and B3LYP methods at 1047, 1031 cm^{-1} and 1041 (81%), 1007 (72%) cm^{-1} respectively for CH_3 rocking vibration exactly coincide with literature as well as recorded spectrum. The

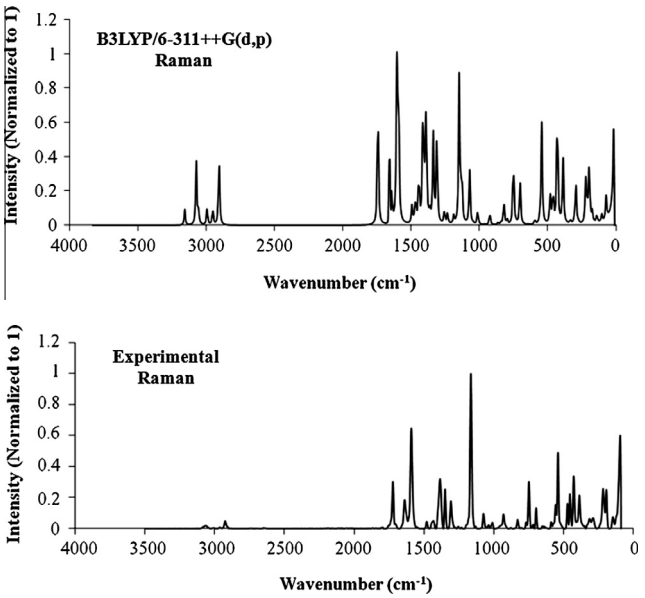

Fig. 4. Comparison of observed and calculated FT-Raman spectra of 8-formyl-7-hydroxy-4-methylcoumarin.

CH_3 torsional mode is observed at 150 cm^{-1} in FT-Raman. The theoretical results corresponding to this vibration are predicted at 165 cm^{-1} and 166 cm^{-1} by HF and B3LYP methods respectively.

4.2.3. C=O and C–O vibrations

Almost all carbonyl compounds have a very intense and narrow peak in the range of 1800–1600 cm^{-1} [53,55] or in other words the carbonyl stretching frequency has been most extensively studied by infrared spectroscopy. Coumarins have two characteristic strong absorption bands arising from C=O and C–O stretching vibrations. The intense C=O stretching vibrations occurs at higher frequencies than that normal ketons. In our present study, a very strong band at 1746 cm^{-1} in FT-IR and 1726 cm^{-1} as a strong band in FT-Raman spectrum are readily assigned to the C=O vibration of coumarin; the corresponding HF and DFT computed mode at 1808 and 1736 (82%) cm^{-1} respectively, is good agreement with the observed as well as related work [25,29]. The DFT value is in good agreement with experimental data than HF value.

The wave number computed at 1735, 1667 cm^{-1} (mode no. 10) by HF/6-311++G(d,p) and B3LYP/6-311G++(d,p) level respectively, are assigned to the C=O stretching vibration of formyl group, and the corresponding experimental bands in IR and Raman are at 1647 and 1642 cm^{-1} respectively. The computed wave numbers at 1321, 1078 and 918 cm^{-1} (mode Nos. 22, 29 and 34) by HF method and 1333, 1065 and 917 cm^{-1} by B3LYP method are assigned to C–O stretching vibrations, the PEDs corresponding to these modes are 51%, 65% and 58% respectively, and shows good agreement with the recorded values at 1300 and 1074 cm^{-1} in FT-IR spectrum and 1310 and 1077 cm^{-1} in FT-Raman spectrum.

4.2.4. Ring system vibrations

The C–C ring stretching vibrations are expected within the region 1650 to 1200 cm^{-1}. In general, the bands are of variable intensity and are observed at 1625–1590, 1575–1590, 1470–1540, 1430–1465 and 1280–1380 cm^{-1} from the frequency ranges given by Varsanyi [52] for the five bands in the region. Most of the ring modes are altered by the substitution to aromatic ring. The actual position of these modes determined not so much by the natural of the substituent but by the form of substitution around the ring system [57]. In the present study the frequency bands at 1595, 1480, 1184 and 1167 cm^{-1} in FTIR spectrum and at 1594, 1484 and 1167 cm^{-1} in FT-Raman are assigned to C–C stretching vibrations for molecule 8-formyl-7-hydroxy-4-methylcoumarin. The theoretically computed wave number also present consistent agreement with experimental observation at 1655, 1612, 1592, 1487, 1437, 1245, 1173 and 1124 cm^{-1} by HF method and at 1637, 1600, 1588, 1489, 1438, 1306, 1182 and 1141 cm^{-1} by B3LYP method. The PED lies between 35% and 57%. The C–C–C inplane bending vibrations are observed at 773, 696, and 455 cm^{-1} in FT-IR and 772, 700, 457 and 317 cm^{-1} in FT-Raman. The in plane bending vibrations are calculated by B3LYP method at 790, 695, 453, 380, 326 and 286 cm^{-1} with PED contribution between 52% and 71%.

The relationship between the experimental and computed DFT/B3LYP frequencies is shown in Supplementary Fig. S1. As shown in Table 2, Supplementary Table S1 and Fig. S1, B3LYP/6-311++G(d,p) computed values show better agreement with the experimental values.

4.3. Natural bond orbital (NBO) analysis

The natural bond orbital analysis provides an efficient method for studying intra and intermolecular bonding and interaction among bonds, and also provides a convenient basis for investigating charge transfer or conjugative interaction in molecular systems. Stabilizing interactions between filled and unoccupied orbitals and destabilizing interactions between filled orbitals can also be obtained from this analysis [58]. The second order Fock matrix was carried out to evaluate the donor–acceptor interactions in the NBO analysis [59]. For each donor NBO (i) and acceptor NBO (j), the stabilization energy associated with $i \rightarrow j$ delocalization can be estimated as,

$$E(2) = \Delta E_{ij} = q_i \frac{F(i,j)^2}{\varepsilon_i \varepsilon_j}$$

where q_i is the donor orbital occupancy, ε_i and ε_j are diagonal elements (orbital energies) and $F(i, j)$ is the off-diagonal Fock matrix element. The larger $E(2)$ value, the more intensive is the interaction between electron donors and acceptors, i.e. the more electrons donating tendency from electron donors to acceptors and greater the extent of conjugation of the whole system. NBO analysis has been performed on the 8-formyl-7-hydroxy-4-methylcoumarin at the DFT/B3LYP/6-311++G(d,p) level in order to elucidate the intramolecular interaction, rehybridization and delocalization of electron density within the molecule. The most important interactions between Lewis, non-Lewis orbitals and O lone pairs, the second order perturbation energy values, E(2), corresponding to these interactions, and the change in electron density (ED) in the σ^* and π^* antibonding orbitals have been shown in Supplementary Table S2. The intramolecular hyperconjugative interactions are formed by the orbital overlap between σ and π (C–C, C–O, C–H and O–H) and σ^* and π^* (C–C, C–O, C–H and O–H) bond orbitals which results ICT (Intra molecular charge transfer) causing stabilization of the system. These interactions are observed as increase in electron density (ED) in C–C, C–O, C–H and O–H antibonding orbitals that weakens the respective bonds.

The strong intramolecular conjugative interaction of the π electrons from C_9–C_{10} to the antibonding orbital of C_3–C_4 and C_5–C_6 bonds shows an ED of ~1.61e, leading to the stabilization energy of 18.08 and 22.05 kJ mol^{-1} respectively, this enhanced $\pi^*(C_9$–$C_{10})$ NBO further conjugates with $\pi^*(C_3$–$C_4)$ and $\pi^*(C5$–$C_6)$ resulting in an enormous stabilization energy of 87.04 and 221.39 kJ/mol respectively. Similarly, another intramolecular conjugative interaction of the π electrons from C_2–O_{11} to $\pi^*(C_3$–$C_4)$ leading to the stabilization energy of 5.09 kJ mol^{-1}. This enhanced $\pi^*(C_2$–$O_{11})$ NBO further conjugates with $\pi^*(C_3$–$C_4)$ resulting in an enormous stabilization energy of 100.21 kJ/mol.

As well as the hyperconjugative interactions of the $\sigma \rightarrow \sigma^*$ or π^* transitions occur from various bonds in our molecule; particularly, σ (C_{14}–H_{23}) having the bigger energetic contribution of their anti-bonding σ^* (C_{14}–O_{15}) and π^* (C_{14}–O_{15}) interactions at 46.48 and 137.17 kJ mol^{-1}, respectively. The other important intramolecular charge transfer in 8-formyl-7-hydroxy-4-methylcoumarin from π (C_3–C_4) with ED of ~1.80e, to π^* (C_2–O_{11}) and π^*(C_9–C_{10}) antibonding orbitals with stabilization energy of 25.33 and 10.06 kJ mol^{-1}, respectively and from σ (C_8–C_{14}) to π^* (C_{14}–O_{15}) with stabilization energy of 48.56 kJ mol^{-1} are listed in Supplementary Table S2.

The most important interaction ($n \rightarrow \sigma^*$) energies, related to the resonance in the molecule, are electron donation from the LP(2) O_{11} atom of the electron donating group to the anti-bonding acceptor σ^* (O_1–C_2) and σ^* (C_2–C_3) of the pyrone ring with stabilization energy of 41.09 and 15.51 kJ/mol, respectively. Another strong interactions have been observed between the p-type orbital containing the lone LP(2) of O_1 and the neighbor π^* (C_2–O_{11}) and π^* (C_9–C_{10}) antibonding orbitals, which leads to a strong stabilization energies of 30.87 and 34.05 kJ/mol. This interaction is responsible for a pronounced decrease of the lone pair orbital occupancy (1.74042), than the other occupancy and hence there is a possibility for delocalization of lone pair of electrons between O_1 and C_9–C_{10}. Also, the strong interaction observed between the lone LP(2) of O_{15} and the anti-bonding acceptor σ^* (O_{13}–H_{22}) of hydroxyl group with stabilization energy of 17.98 kJ/mol, confirm the presence of an intramolecular interaction between the hydrogen (H_{22}) and the formyl oxygen atom (O_{15}).

The natural atomic charge calculation has an important role in the application of quantum chemical calculation to molecular system because of atomic charges effect dipole moment, molecular polarizability, electronic structure and more a lot of properties of molecular systems [60,61]. The net charge distribution of 8-formyl-7-hydroxy-4-methylcoumarin was calculated by the Mulliken and NBO methods with HF/6-311G++(d,p) and B3LYP/6-311G++(d,p) basis sets and the charges are listed in Supplementary Table S3. In the present study, the positive charge distribution over the hydrogen atoms and the negative NBO charge distribution in the other atoms except C_2, C_4, C_7, C_9 and C_{14}. The maximum atomic NBO charge is obtained for C_2 when compared with other atoms. This is due to the attachment of negatively charged carbon (C_3) and oxygen atoms (O_1 and O_{11}). In addition, the O_{13} oxygen atom has large negative NBO charge than the other oxygen atoms and behaves as electron acceptor. The carbon atom C_{12} is more negative than the other carbon atoms due to electron-delocalization of π-electrons between the γ-CH_3 and carbonyl of the pyrone, which increases the double bond character of the bonds joining them (see Supplementary Table S3).

4.4. Frontier molecular orbitals (FMOs)

Molecular orbitals and their properties such as energy are very useful for physicists and chemists and are very important parameters for quantum chemistry. The most important orbitals in a molecule are the frontier molecular orbitals, called highest occupied molecular orbital (HOMO) and lowest unoccupied molecular orbital (LUMO). Both the highest occupied molecular orbital and lowest unoccupied molecular orbital are the main orbital take part in chemical stability [62]. The HOMO represents the ability to donate an electron, LUMO as an electron acceptor represents the ability to obtain an electron. In order to evaluate the energetic behavior of the title compound, we carried out calculations in vacuo and in organic solvent (chloroform). The total energy, HOMO−1, HOMO, LUMO and LUMO+1 energies, the energy gap, the dipole moment (D), the ionization potential (I), the electron affinity (A), the absolute electronegativity (χ), the absolute hardness (η) and softness (S) for the 8-formyl-7-hydroxy-4-methylcoumarin have been calculated at B3LYP/6-311G++(d,p) basis set and the results are given in Supplementary Table S4. 3D plots of the HOMO-1, HOMO, LUMO and LUMO+1 orbitals computed in chloroform at the B3LYP/6-311G++(d,p) level for title molecule are illustrated in Supplementary Fig. S2. The positive phase is red and the negative one is green.

It is clear from the Supplementary Fig. S2 that, the HOMO and LUMO are localized on almost the whole molecule. But, while the HOMO-1 is localized on the benzene ring, LUMO+1 is localized on almost the pyrone ring. Both the HOMOs and the LUMOs are mostly π-anti-bonding type orbitals. The calculated energy value of HOMO is −6.77690 and −6.70343 and LUMO is −2.70042 and −2.63375 eV in gas and chloroform, respectively. Also, the value of energy separation between the HOMO and LUMO is −4.07648 and −4.06968 eV in gas and chloroform, respectively (Supplementary Table S4). Recently, the energy gap between HOMO and LUMO has been used to prove the bioactivity from intra-molecular charge transfer (ICT) [63,64], and describes the chemical reactivity, optical polarizability, kinetic stability, and chemical softness-hardness of a molecule. By using HOMO and LUMO energy values for a molecule, electronegativity and chemical softness–hardness can be calculated as follows [65]:

$$\chi = \frac{(I+A)}{2}; \eta = \frac{(I-A)}{2}; S = \frac{1}{2\eta} \text{ where } I = -E_{HOMO} \text{ and } A = -E_{LUMO}.$$

The chemical hardness is a good indicator of the chemical stability. The molecules having a small energy gap are known as soft and having a large energy gap are known as hard molecules. Earlier studies have reported that hardness (η) and softness (S), other than the electron-accepting and -donating properties are important factors in estimating the cytotoxic activity of coumarin derivatives [66,67]. Recently, Gacche and Jadhav have reported that lower calculated η for coumarin derivatives showing relatively lower cytotoxicity [68]. Therefore, 8-formyl-7-hydroxy-4-methylcoumarin with absolute hardness of 2.03824 eV can be considered as a lead molecule for maneuvering novel cytotoxic agents. The dipole moment in a molecule is another important electronic property which results from non-uniform distribution of charges on the various atoms in a molecule. Based on predicted dipole moment values, one can say that in going from the gas phase to the solvent phase, the dipole moment value increases (Supplementary Table S4).

4.5. Molecular Electrostatic Potential (MEP)

The Molecular Electrostatic Potential (MEP) is a plot of electrostatic potential mapped onto the constant electron density surface. The MEP has been used primarily for predicting sites and relative reactivities towards electrophilic attack, in studies of biological recognition and hydrogen bonding interactions [69,70]. The different values of the electrostatic potential at the surface are represented by different colors; red represents regions of most

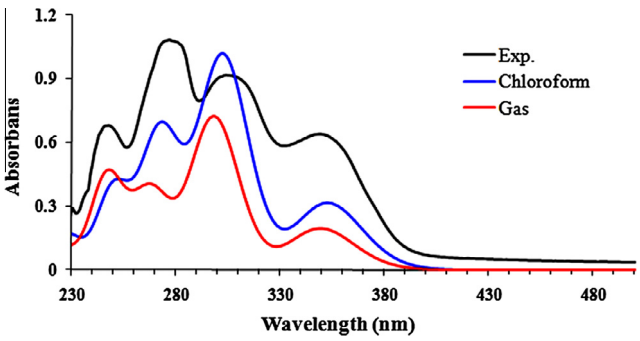

Fig. 5. Experimental and calculated UV–vis spectra of title compound.

Table 3
Experimental and calculated absorption wavelength λ (nm), excitation energies E (eV) and oscillator strengths (f) of 8-formyl-7-hydroxy-4-methylcoumarin.

Experimental			TD-DFT/B3LYP/6-311++G(d,p)						Symmetry	Major contribution[a]
$CHCl_3$			Gas			$CHCl_3$				
λ(nm)	E(eV)	Abs.	λ (nm)	E (eV)	f (a.u.)	λ (nm)	E (eV)	f (a.u.)		
350	3.5429	0.638	349.24	3.5506	0.0671	352.69	3.5158	0.1082	Singlet-A′	HOMO → LUMO (90%)
304	4.0789	0.916	298.21	4.1581	0.2479	302.57	4.0982	0.3469	Singlet-A′	HOMO → L + 1 (92%)
276	4.4928	1.079	268.19	4.6236	0.1295	272.91	4.5436	0.2294	Singlet-A′	H-1 → LUMO (91%)
248	5.0000	0.679	247.16	5.0170	0.1540	250.45	4.9511	0.1342	Singlet-A′	H-1 → L + 1 (92%)

[a] H: Homo, L: Lumo.

negative electrostatic potential (preferred site for electrophilic attack), blue represents regions of most positive electrostatic potential (preferred site for nucleophilic attack) and green represents regions of zero potential. Potential increases in the order red < orange < yellow < green < blue. To predict reactive sites for electrophilic and nucleophilic attack for 8-formyl-7-hydroxy-4-methylcoumarin, the MEP at the B3LYP/6-311++G(d,p) method was calculated and 3D plots of MEP is illustrated in Supplementary Fig. S3. The colour code of this map is in the range between −0.1040 a.u. (deepest red) and 0.1040 a.u. (deepest blue) in the title compound. As can be seen from the MEP map of the molecule, the negative region is mainly localized from carbonyl and hydroxyl group whereas the positive region is lies in the hydrogen and partially over the ring system.

4.6. UV–vis spectral analysis

All molecules allow strong σ–σ^* and π–π^* transitions in the UV–vis region with high extinction coefficients [71]. The electronic absorption spectrum of the title compound in chloroform solvent is recorded within the 230–500 nm range and shown in Fig. 5. In order to support our experimental observations, TD-B3LYP/6-311++G(d,p) calculations on electronic absorption spectra in vacuum and chloroform solution were performed. The experimental peaks together with the calculated excitation energies, oscillator strength (f), absorption wavelength (λ) and major contributions of the transitions were given in Table 3. GaussSum 2.2 Program [72] has been used to calculate the major contributions of the transitions and prepare the simulated UV–vis spectrum of title compound in gas phase and chloroform solution as shown in Fig. 5.

Calculations of the molecular orbital geometry show that the visible absorption maxima of this molecule correspond to the electron transition between frontier orbitals such as translation from HOMO to LUMO. Due to the Frank-Condon principle, the maximum absorption peak (λ max) in an UV–visible spectrum corresponds to vertical excitation. As can be seen from Table 3, the B3LYP/6-311G++(d,p) calculations (in chloroform) predict four intense electronic transitions at 352.69, 302.57, 272.91 and 250.45 nm with oscillator strength of 0.1082, 0.3469, 0.2294 and 0.1342 respectively, which are in excellent agreement with the measured experimental data (350, 304, 276 and 248 nm). In view of calculated absorption spectra, the maximum absorption wavelength corresponds to the electronic transition from the HOMO to LUMO with 90% contribution. The other wavelength and calculated counterparts with major contributions can be seen in Table 3. As can be seen from Table 3, calculations performed at $CHCl_3$ and gas phase are close to each other.

4.7. NMR spectral analysis

NMR spectroscopy has proved to be an exceptional tool to elucidate structure and molecular conformation. In order to provide an unambiguous assignment and analysis ^1H and ^{13}C NMR spectra, theoretical calculations on chemical shift of 8-formyl-7-hydroxy-4-methylcoumarin were done by Gauge Independent Atomic

Table 4
Calculated ($\delta_{Theo.}$) and experimental ($\delta_{Exp.}$) ^1H and ^{13}C NMR chemical shifts for the title molecule.

Atom	Experimental	HF/6-311++G(d,p)			B3LYP/6-311++G(d,p)		
		Gas phase	$CHCl_3$	$\lvert\delta_{Exp} - \delta_{Theo}\rvert$	Gas phase	$CHCl_3$	$\lvert\delta_{Exp} - \delta_{Theo}\rvert$
H(16)	6.129	5.944	6.091	0.038	6.062	6.235	0.106
H(17)	2.363	2.224	2.375	0.012	2.073	2.217	0.146
H(18)	2.363	2.314	2.477	0.114	2.351	2.489	0.126
H(19)	2.363	2.314	2.477	0.114	2.351	2.489	0.126
H(20)	7.675	7.970	8.345	0.670	7.561	7.875	0.200
H(21)	6.837	6.926	7.077	0.240	6.896	7.053	0.216
H(22)	12.118	10.160	10.083	2.035	13.101	12.926	0.808
H(23)	10.528	10.592	10.602	0.074	11.030	10.986	0.458
$\delta_{Exp} = 0.937\ \delta_{Theo} + 0.173$			$R^2 = 0.9988$	RMSD = 0.139	For B3LYP method in $CHCl_3$		
C(2)	156.085	160.110	165.164	9.079	161.906	165.947	9.862
C(3)	111.997	112.773	111.266	0.731	116.872	116.547	4.55
C(4)	152.773	162.111	168.060	15.287	158.869	163.851	11.078
C(5)	133.008	145.372	148.722	15.714	137.620	140.828	7.82
C(6)	114.268	114.110	114.739	0.471	119.169	120.269	6.001
C(7)	165.195	175.667	175.835	10.64	175.489	175.652	10.457
C(8)	108.599	108.500	108.607	0.008	114.326	114.728	6.129
C(9)	159.199	165.834	165.959	6.760	167.670	167.485	8.286
C(10)	112.360	108.414	110.114	2.246	117.006	118.623	6.263
C(12)	18.973	19.998	20.500	1.527	21.232	21.761	2.788
C(14)	193.363	195.691	198.607	5.244	200.586	202.419	9.056
$\delta_{Exp} = 0.953\ \delta_{Theo} - 1.024$			$R^2 = 0.9993$	RMSD = 1.317	For B3LYP method in $CHCl_3$		

Orbital (GIAO) method at HF/6-311++G(d,p) and B3LYP/6-311++G(d,p) level in gas and $CHCl_3$ solution. The ^{13}C and ^{1}H theoretical and experimental chemical shifts, isotropic shielding tensors and the assignments of 8-formyl-7-hydroxy-4-methylcoumarin are presented in Table 4. The experimental ^{1}H and ^{13}C NMR spectra are shown in Supplementary Figs. S4 and S5 respectively. We have calculated ^{1}H chemical shift values (with respect to TMS) of 2.224–10.592 ppm and 2.073–13.101 ppm in gas phase and values of 2.375–10.602 ppm and 2.217–12.926 ppm in chloroform solution at HF and B3LYP level respectively, whereas the experimental shifts are observed at 2.363–12.118 ppm. The characteristic downfield signal at δ 12.118 ppm is attributed to the hydroxyl proton (H_{22}). The electronegative oxygen atom (O_{15}) present in the carbon atom (C_{14}) deshields the proton (H_{22}) by means of a strong intramolecular hydrogen bonding (O_{13}–$H_{22}\cdots O_{15}$) which reduces the electron density on H_{22} resulted in downfield chemical shift. The downfield signal at δ 10.528 ppm corresponds to proton of formyl group (H_{23}). The aromatic protons and the olefinic proton of heterocyclic ring appeared downfield signals at δ values 6.129, 6.837 and 7.675 ppm for protons H_{16}, H_{21} and H_{20}, respectively. In addition, the upfield signal at δ 2.363 ppm corresponds to protons of methyl group.

Aromatic carbons give signals in overlapped areas of the spectrum with chemical shift values from 100 to 200 ppm [73,74]. In our present investigation, the calculated ^{13}C chemical shift values (with respect to TMS) are in the range of 19.998–195.691 ppm and 21.232–200.586 ppm in gas phase and values of 20.500–198.607 ppm and 21.761-202.419 ppm in chloroform solution at HF and B3LYP level respectively, whereas the experimental shifts are observed at 18.973–193.363 ppm.

The largest deviations between the calculated and experimental ^{13}C NMR chemical shifts ($|\delta_{Exp} - \delta_{Theo}|$) observed for C_4 with 11.078 at B3LYP/6-311++G(d,p) level. The chemical shift values observed at 193.363 and 156.085 ppm are assigned to carbonyl of formyl and the pyrone ring respectively. The carbonyl of pyrone ring appeared at upfield signal than formyl group, due to the delocalization of the lone pair electrons from O_1 to the C=O. The chemical shifts of the benzene ring carbon atoms C_5, C_6, C_7, C_8, C_9 and C_{10} are assigned to 133.008, 114.268, 165.195, 108.599, 159.199 and 112.360 ppm respectively. Due to the more electronegative oxygen atoms (O_1 and O_{13}) in ring, the chemical shift of the C_7 and C9 carbon atoms in benzene ring are set to downfield. The C_3 carbon atom is highly shielded than C_4 due to the delocalization of the lone pair electrons from C_2=O_{11} group to the adjacent C_4=C_3. Therefore, the chemical shift of C_4 is observed at the downfield at 152.773 ppm, whereas the chemical shift of C_3 is observed at 111.997 ppm. Moreover, the observed upfield signal at δ 18.973 ppm is assigned to methyl group. As can be seen from Table 4, the calculated chemical shifts are in good agreement with the experimental values. The correlation graphics between the experimental and calculated ^{1}H NMR and ^{13}C NMR chemical shifts of 8-formyl-7-hydroxy-4-methylcoumarin are presented in Supplementary Fig. S6 and Fig S7.

4.8. Thermodynamic properties

The thermodynamic data supply helpful information for evaluate the amount of energy released or absorbed in a chemical reaction according to the second law of thermodynamics in thermochemical field [75] and to calculate other thermodynamic functions, such as Gibbs energies and equilibrium constants, and more importantly, they permit a quantitative assessment of the relative stability of a molecule. The prediction of the behavior and reaction kinetics of organic compounds requires an accurate description of their thermochemical properties. In this regard, estimation methods, ab initio quantum mechanical methods, and more recently, density functional theory (DFT) calculations have been used as an independent confirmation of the accuracy of the experimental measurements and often because of lack of available experimental data. In the present study, the standard statistical thermodynamic functions such as heat capacity ($C^0_{p,m}$), entropy (S^0_m) and enthalpy changes (H^0_m) for the 8-formyl-7-hydroxy-4-methylcoumarin were calculated at B3LYP/6-311++G(d,p) level in gas phase from the theoretical harmonic frequencies and the results presented in Supplementary Table S5. As observed from Supplementary Table S5, the values $C^0_{p,m}$, S^0_m and H^0_m all increase with the increase of temperature from 100 to 600 K, which is attributed to the enhancement of the molecular vibration as the temperature increases [75]. The correlation equations between heat capacity, entropy, enthalpy changes and temperatures were fitted by quadratic formulas, and the corresponding fitting factors (R^2) for these thermodynamic properties are 0.99998, 0.99983 and 0.99991, respectively. The corresponding fitting equations are as follows and the correlation graphics of those are shown in Supplementary Figs. S8–S10.

$$S^0_m = 53.3614 + 0.1983T - 5.1632T^2 (R^2 = 0.99998)$$
$$C^0_{p,m} = 0.3871 + 0.1822T - 7.9604T^2 (R^2 = 0.99983)$$
$$H^0_m = -0.5147 + 0.0104T + 6.3972T^2 (R^2 = 0.99991)$$

5. Conclusion

In summary, the 8-formyl-7-hydroxy-4-methylcoumarin has been synthesized in two step starting from resorcinol, and characterized by elemental analysis, ^{1}H, ^{13}C NMR, UV, FT-IR and FT-Raman spectroscopy. The vibrational bands observed in FT-infrared and FT-Raman spectra of this compound were assigned based on the potential energy distribution (PED) and supported by theoretically calculated (scaled) DFT and HF vibrational spectra. The comparison of the experimental and calculated spectra of the title molecule showed that calculated scaled frequencies obtained using the DFT/6-311++G(d,p) method is in good agreement with experimental results. NBO analysis shows that charge transfer mainly due to C–C group and shows interaction between the 'filled' donor-type NBO and 'empty' acceptor-type NBO in the molecule and their stabilization energies are estimated by second order Fock matrix. The intramolecular charge transfer in 8-formyl-7-hydroxy-4-methylcoumarin from π (C_3–C_4) to π* ($C2$–O_{11}) has the stabilization energy of 25.33 kJ mol^{-1}. The lowering of HOMO–LUMO energy gap clearly explains the charge transfer interactions taking place within the molecule. GIAO NMR calculations provided chemical shift values that were in good agreement with experimental data. Furthermore, the excellent agreement has been observed between the experimental and theoretically absorption wavelength calculated by TD-DFT/6-311++G(d,p) method in gas and $CHCl_3$ solution.

Appendix A. Supplementary material

Supplementary data associated with this article can be found, in the online version, at http://dx.doi.org/10.1016/j.molstruc.2013.08.043.

References

[1] D. Sajan, Y. Erdogdu, R. Reshmy, O. Dereli, K. Kurien Thomas, I. Hubert Joe, Spectrochim. Acta A 82 (2011) 118.
[2] National Toxicology Program Technical Report on the Toxicology and Carcinogenesis of Coumarin in F344/N Rats and B6C3F1 Mice (Gavage Studies). US Department of Health and Human Services, NIH, Publication No. 92-3153, 1992.

[3] D. Egan, R. O'Kennedy, E. Moran, D. Cox, E. Prosser, R.D. Thornes, Drug Metabol. Rev. 22 (1990) 503.
[4] J.R.S. Hoult, M. Paya, Gen. Pharmacol. 27 (1996) 713.
[5] J.W. Suttie, Clin. Cardiol. 13 (1990) 16.
[6] D.A. Egan, P. James, D. Cooke, R.O. Kennedy, Cancer Lett. 118 (1997) 201.
[7] A.M. El-saghier, A. Khodiyar, Sulfur Silicon 160 (2000) 105.
[8] J. Azizian, A. Mohammadi, I. Bidar, P. Mirazaei, Montash Chem. 139 (2008) 805.
[9] C. Gnerre, M. Catto, F. Leonetti, P. Weber, P.A. Carrupt, C. Altomare, A. Carotti, B.J. Testa, J. Med. Chem. 43 (2000) 4747.
[10] L.K.A.M. Leal, A.A.G. Ferreira, G.A. Bezerra, F.J.A. Matos, G.S.B. Viana, J. Ethnopharmacol. 70 (2000) 151.
[11] G. Smitha, R. Sanjeeva, Synth. Commun. 34 (2004) 3997.
[12] N. Hamdi, C. Lidrissi, M. Saoud, A.R. Nievas, H. Zarrouk, Chem. Heterocycl. Com. 42 (2006) 320.
[13] M. Paya, P.A. Goodwin, B. De Las Heras, R.S. Hoult, Biochem. Pharmacol. 48 (1994) 445.
[14] F.P. Schäfer (Ed.), Dye Lasers, third ed., vol. 1, Springer-Verlag, Berlin, New York, 1990, p. 244.
[15] S.W. Hong, W.H. Jo, Polymer 49 (2008) 4180.
[16] N. Saleh, Y.A. Al-Soud, W.M. Nau, Spectrochim. Acta A 71 (2008) 818.
[17] T. Hirano, K. Hiromoto, H. Kagechika, Org. Lett. 9 (2007) 1315.
[18] C. Aliaga, J.M. Juárez-Ruiz, J.C. Scaiano, A. Aspée, Org. Lett. 10 (2008) 2147.
[19] L. Du, M. Li, S. Zheng, B. Wang, Tetrahedron Lett. 49 (2008) 3045.
[20] Ý L. Du, Ý N. Ni, M. Li, B. Wang, Tetrahedron Lett. 51 (2010) 1152.
[21] R.S. Rasmussen, R.R. Brattain, J. Am. Chem. Soc. 71 (1949) 1073.
[22] C.P. Girijavallabhan, K. Venkateswarlu, Curr. Sci. 37 (1968) 11.
[23] S.S. Saleem, G. Aruldhas, Indian J. Pure Appl. Phys. 21 (1984) 110.
[24] S.R. Tripati, N.K. Sanyal, Indian J. Phys. 63B (1989) 474.
[25] A. Ramoji, J. Yenagi, J. Tonannavar, V.B. Jadhav, M.V. Kulkarni, Spectrochim. Acta. A 68 (2007) 504.
[26] V. Sortur, J. Yenagi, J. Tonannavar, V.B. Jadhav, M.V. Kulkarni, Spectrochim. Acta. A 64 (2006) 301.
[27] V. Sortur, J. Yenagi, J. Tonannavar, V.B. Jadhav, M.V. Kulkarni, Spectrochim. Acta. A 71 (2008) 688.
[28] V. Arjunan, R. Santhanam, S. Sakiladevi, M.K. Marchewka, S. Mohan, J. Mol. Struct. 1037 (2013) 305.
[29] N. Udaya Sri, K. Chaitanya, M.V.S. Prasad, V. Veeraiah, A. Veeraiah, Spectrochim. Acta. A 97 (2012) 728.
[30] S. Sebastian, S. Sylvestre, D. Jayarajan, M. Amalanathan, K. Oudayakumar, T. Gnanapoongothai, T. Jayavarthanan, Spectrochim. Acta A 101 (2013) 370.
[31] L. Joseph, D. Sajan, R. Reshmy, B.S. Arun Sasi, Y. Erdogdu, K. Kurien Thomas, Spectrochim. Acta A 99 (2012) 234.
[32] M.S. Manhas, S.N. Ganguly, S. Mukherjee, Tetrahedron Lett. 47 (2006) 2423.
[33] A. Kulkarni, S.A. Patil, P.S. Badami, Eur. J. Med. Chem. 44 (2009) 2904.
[34] M.J. Frisch, G.W. Trucks, H.B. Schlegel, G.E. Scuseria, M.A. Robb, J.R. Cheeseman, G. Scalmani, V. Barone, B. Mennucci, G.A. Petersson, H. Nakatsuji, M. Caricato, X. Li, H.P. Hratchian, A.F. Izmaylov, J. Bloino, G. Zheng, J.L. Sonnenberg, M. Hada, M. Ehara, K. Toyota, R. Fukuda, J. Hasegawa, M. Ishida, T. Nakajima, Y. Honda, O. Kitao, H. Nakai, T. Vreven, J.A. Montgomery Jr., J.E. Peralta, F. Ogliaro, M. Bearpark, J.J. Heyd, E. Brothers, K.N. Kudin, V.N. Staroverov, R. Kobayashi, J. Normand, K. Raghavachari, A. Rendell, J.C. Burant, S.S. Iyengar, J. Tomasi, M. Cossi, N. Rega, J.M. Millam, M. Klene, J.E. Knox, J.B. Cross, V. Bakken, C. Adamo, J. Jaramillo, R. Gomperts, R.E. Stratmann, O. Yazyev, A.J. Austin, R. Cammi, C. Pomelli, J.W. Ochterski, R.L. Martin, K. Morokuma, V.G. Zakrzewski, G.A. Voth, P. Salvador, J.J. Dannenberg, S. Dapprich, A.D. Daniels, O. Farkas, J.B. Foresman, J.V. Ortiz, J. Cioslowski, D.J. Fox, Gaussian, Inc., Wallingford, CT, 2009
[35] A.A. Hakan, Int. J. Mol. Sci. 8 (2007) 760.
[36] N. Sundaraganesan, S. Illakiamani, H. Saleem, P.M. Wojciechowski, D. Michalska, Spectrochim. Acta A 61 (2005) 2995.
[37] M.H. Jamroz, Vibrational Energy Distribution Analysis, VEDA 4, Warsaw, 2004.
[38] R.I. Dennington, T. Keith, J. Millam, GaussView, Version 5.0.8, Semichem. Inc., Shawnee Mission, KS, 2008.
[39] G. Keresztury, S. Holly, J. Varga, G. Besenyei, A.Y. Wang, J.R. Durig, Spectrochim. Acta A 9 (1993) 2007.
[40] G. Keresztury, in: J.M. Chalmers, P.R. Griffith (Eds.), Raman Spectroscopy: Theory, Handbook of Vibrational Spectroscopy, vol. 1, John Wiley & Sons Ltd., New York, 2002.
[41] E.D. Glendening, J.K. Badenhoop, A.E. Reed, J.E. Carpenter, J.A. Bohmann, C.M. Morales, F. Weinhold, NBO 5.0, Theoretical Chemistry Institute, University of Wisconsin, Madison, 2001.
[42] M. Petersilka, U.J. Gossmann, E.K.U. Gross, Phys. Rev. Lett. 76 (1966) 1212.
[43] E. Runge, E.K.U. Gross, Phys. Rev. Lett. 52 (1984) 997.
[44] R. Bauernschmitt, R. Ahlrichs, Chem. Phys. Lett. 256 (1996) 454.
[45] C. Jamorski, M.E. Casida, D.R. Salahub, J. Chem. Phys. 104 (1996) 5134.
[46] R. Ditchfield, J. Chem. Phys. 56 (1972) 5688.
[47] K. Wolinski, J.F. Hinton, P. Pulay, J. Am. Chem. Soc. 112 (1990) 8251.
[48] H. Yuvaraj, D. Gayathri, R.G. Kalkhambkar, G.M. Kulkarni, R.M. Bapsetd, Acta Crystallogr. Sect. E Struct. Rep. 67 (2011) o1513.
[49] D. Michalska, D.C. Bienko, A.J.A. Bienko, Z. Latajaka, J. Phys. Chem. 100 (1996) 17786.
[50] V. Krishnakumar, S. Muthunatesan, Spectrochim. Acta A 65 (2006) 818.
[51] V. Krishnakumar, V. Balachandran, T. Chithambarathanu, Spectrochim. Acta A 62 (2005) 918.
[52] G. Varsanyi, Vibrational Spectra of Benzene Derivatives, Academic Press, New York, 1969.
[53] V. Krishnakumar, R. John Xavier, Indian J. Pure Appl. Phys. 41 (2003) 597.
[54] B.C. Smith, Infrared Spectral Interpretation: A Systematic Approach, CRC Press, Boca Raton, Florida, 1998.
[55] G. Socrates, Infrared and Raman Characteristic Group Frequencies – Tables and Charts, third ed., John Wiley & Sons, Chichester, 2001.
[56] N.P.G. Roeges, A Guide to the Complete Interpretation of Infrared Spectra of Organic Structures, Wiley, New York, 1994.
[57] L.J. Bellamy, The Infrared Spectra of Complex Molecules, Wiley, New York, 1959.
[58] H.W. Thomson, P. Torkington, J. Chem. Soc. 171 (1945) 640.
[59] M. Szafram, A. Komasa, E.B. Adamska, J. Mol. Struct. 827 (2007) 101.
[60] R. Meenakshi, Mol. Simulat. 36 (2010) 425.
[61] I. Sidir, Y.G. Sidir, M. Kumalar, E. Tasal, J. Mol. Struct. 964 (2010) 134.
[62] S. Gunasekaran, R.A. Balaji, S. Kumeresan, G. Anand, S. Srinivasan, Can. J. Anal. Sci. Spectrosc. 53 (2008) 149.
[63] L. Padmaja, C. Ravi Kumar, D. Sajan, I. Hubert Joe, V.S. Jayakumar, G.R. Pettit, J. Raman Spectrosc. 40 (2009) 419.
[64] S. Sagdinc, H. Pir, Spectrochim. Acta A73 (2009) 181.
[65] R.G. Pearson, Proc. Natl. Acad. Sci. 83 (1986) 8440.
[66] S. Kobayashi, K. Sameshima, Y. Ishii, A. Tanaka, Chem. Pharm. Bull. 43 (1995) 1780.
[67] S. Kobayashi, H. Hamashima, M. Kurihara, N. Miyata, A. Tanaka, Chem. Pharm. Bull. 46 (1998) 1108.
[68] R.N. Gacche, S.G. Jadhav, J. Exp. Clin. Med. 4 (2012) 165.
[69] J.S. Murray, K. Sen, Molecular Electrostatic Potentials, Concepts and Applications, Elsevier, Amsterdam, 1996. pp. 7–624.
[70] E. Scrocco, J. Tomasi, Adv. Quantum Chem. 11 (1978) 115.
[71] R.M. Silverstein, G.C. Bassler, T.C. Morrill, Spectrometric Identification of Organic Compounds, John Wiley, Chichester, 1991.
[72] N.M. O' Boyle, A.L. tenderholt, K.M. Langer, J. Comput. Chem. 29 (2008) 839.
[73] K. Pihlaja, E. Kleinpeter (Eds.), Carbon-13 Chemical Shifts in Structural and Sterochemical Analysis, VCH Publishers, Deerfield Beach, 1994.
[74] Y.R. Sharma, Elementary Organic Spectroscopy, S. Chand, New Delhi, 2006.
[75] J. Bevan Ott, J. Boerio-Goates, Chemical Thermodynamics: Principles and Applications, Academic Press, San Diego, 2000.